Article

Chinese Science Bulletin

Physical Chemistry

January 2013 Vol.58 No.1: 84–91

doi: 10.1007/s11434-012-5367-9

Visible-light-driven Ag/Ag_3PO_4-based plasmonic photocatalysts: Enhanced photocatalytic performance by hybridization with graphene oxide

ZHU MingShan, CHEN PengLei* & LIU MingHua*

Beijing National Laboratory for Molecular Science, CAS Key Laboratory of Colloid, Interface and Chemical Thermodynamics, Institute of Chemistry, Chinese Academy of Sciences, Beijing 100190, China

Received May 3, 2012; accepted June 14, 2012; published online September 16, 2012

An efficient visible-light-driven plasmonic photocatalyst with regard to graphene oxide (GO) hybridized Ag/Ag_3PO_4 (Ag/Ag_3PO_4/GO) nanostructures has been facilely synthesized via a deposition-precipitation method. The synthesized nanostructures have been characterized by means of scanning electron microscopy (SEM), energy-dispersive X-ray spectroscopy (EDX), X-ray diffraction (XRD), UV-vis spectra, Fourier transform infrared spectra (FT-IR), X-ray photoelectron spectroscopy (XPS), and Raman spectra. It has been disclosed that compared with the bare Ag/Ag_3PO_4 nanospecies, the GO hybridized nanostructures display enhanced photocatalytic activity for the photodegradation of methyl orange pollutant under visible-light irradiation. It is suggested that the reinforced charge transfer and the suppressed recombination of electron-hole pairs in Ag/Ag_3PO_4/GO, the smaller size of Ag/Ag_3PO_4 nanospecies in Ag/Ag_3PO_4/GO, all of which are the consequences of the hybridization of GO, are responsible for the enhanced photocatalytic performance. The investigation might open up new opportunities to obtain highly efficient Ag_3PO_4-based visible-light-driven plasmonic photocatalyst for the photodegradation of organic pollutants.

plasmonic photocatalyst, Ag/Ag_3PO_4, graphene oxide, visible light, photodegradation

Citation: Zhu M S, Chen P L, Liu M H. Visible-light-driven Ag/Ag_3PO_4-based plasmonic photocatalysts: Enhanced photocatalytic performance by hybridization with graphene oxide. Chin Sci Bull, 2013, 58: 84–91, doi: 10.1007/s11434-012-5367-9

Nowadays, most of advanced industrialized nations are faced with tremendous environmental problems associated with organic pollutants and toxic water pollutants [1–3]. To eliminate these pollutants and to purify water, various sophisticated biologically- or physically-based methods such as bio-degradation, adsorption, ultrafiltration, coagulation etc., have been developed. However, in most of the cases, these methods are slow, ineffective and not environmentally compatible [3,4]. In order to address these problems, extensive investigations have been carried out to develop diverse efficient, and environmentally-friend photocatalysts to achieve the photodegradation of the organic pollutants. By now, a paramount of semiconductor-based photocatalysts, traditionally represented by TiO_2-involved nanocomposites, have been investigated to meet the requirements of water purification and pollutant elimination [1–8]. Nevertheless, UV light, which merely accounts for no more than 5% of solar energy, is generally required for the operation of such conventional photocatalysts. This, to a great extent, limits the extensive application possibilities of this kind of photocatalysts [3]. Compared with UV light, it has been recognized that visible light, which accounts for ca. 45% of solar energy, is more attractive for the performance of the photocatalysts [3]. As a consequence, to satisfy the rising demands of the environmental problems, it is currently a topic of general concern to develop visible-light-driven yet highly efficient photocatalysts for the degradation of organic pollutants [3].

Recently, in contrast to the traditional UV-light-driven photocatalysts, visible-light-energized photocatalysts in terms of AgX-based nanospecies have been demonstrated to be one of the most promising alternatives [9–13]. Thus far,

*Corresponding authors (email: chenpl@iccas.ac.cn; liumh@iccas.ac.cn)

numerous AgX-involved photocatalysts, such as Ag/AgCl, Ag/AgBr, etc., have been developed. However, it is still an important issue to initiate more varied opportunities to produce new type visible-light-energized photocatalysts [3,14]. More recently, it has been reported that silver orthophosphate (Ag_3PO_4) could be used as highly active visible-light photocatalyst for the photodegradation of organic pollutants [15]. To further enhance photocatalytic activity of this novel material, great efforts have been addressed in terms of morphology-control [16], size-control [17], and hybridization [18,19]. Nevertheless, besides these efforts, it is highly desirable to develop unique yet highly efficient Ag_3PO_4-based photocatalysts with enhanced photocatalytic activity to provide more varied and new opportunities for pollutant elimination, and to match the requirements of the future environmental issues.

Graphene oxide (GO) has been reported to be an excellent hybridization component for various advanced functional nanocomposites [20–22]. Thus far, a paramount of GO involved nanohybrids have been developed aiming at manufacturing high-efficiency catalyst, especially those for the photodegradation of pollutants [23–31]. On the basis of these backgrounds, it is strongly expected that enhanced photocatalytic performance of Ag_3PO_4 nanospecies might be realized by hybridization with GO nanosheet, which is a nanomaterial of general and broad interest [20–22].

In this paper, we report our new endeavors to produce GO hybridized Ag/Ag_3PO_4 nanomaterials (Ag/Ag_3PO_4/GO) via a deposition-precipitation method. We have showed that the obtained Ag/Ag_3PO_4/GO nanospecies could display a broad plasmonic absorption in a wide range of visible-light region. In terms of photodegradation of methyl orange (MO) pollutant under visible light irradiation, we have demonstrated that compared with the bare Ag/Ag_3PO_4 nanospecies, the GO-involved nanocomposite could display distinctly enhanced photocatalytic performance. On the basis of our experimental facts, an explanation has been proposed for this significant phenomenon. To the best of our knowledge, this might be the first report concerning the assembly of GO hybridized Ag_3PO_4-based nanostructures with enhanced photocatalytic activity. Our exploratory work likely initiates new possibilities for the fabrication of high-efficiency Ag_3PO_4-based visible-light-driven plasmonic photocatalyst with distinctly enhanced photocatalytic performance.

1 Experimental

1.1 Materials and chemicals

Silver acetate (CH_3COOAg, Alfa Aesar, >99%), disodium hydrogen phosphate (Na_2HPO_4, Beijing Chemical Works, >99%), and graphite powder (Alfa Aesar, 325 mesh, 99.9995%) were used as received without further treatments.

1.2 Synthesis of graphene oxide (GO) nanosheets

GO nanosheets were synthesized through the chemical exfoliation of graphite powder by using a modified Hummers' method. The detailed synthesis procedure was carried out according to the methods that described previously [28].

1.3 Synthesis of Ag/Ag_3PO_4 and GO hybridized Ag/Ag_3PO_4 nanostructures

In a typical process, a 500 μL aqueous solutions of GO nanosheet (1 mg mL^{-1}) was added dropwise into a 10 mL aqueous solution of CH_3COOAg (0.01 mol L^{-1}) within 5 min under vigorous magnetic stirring. The stirring was maintained for another 10 min. Subsequently, a 500 μL aqueous solution of Na_2HPO_4 (0.067 mol L^{-1}) was added dropwise into the above aqueous solution within 5 min under vigorous magnetic stirring. The stirring was maintained for another 20 min, after which a brown dispersion containing Ag/Ag_3PO_4/GO hybrid nanocomposite was obtained. The obtained brown solids were collected by centrifugation (10000 r min^{-1}, 10 min), and washed thoroughly with ultrapure Milli-Q water by repeating centrifugations. When only silver acetate species but no GO nanosheets were involved during the synthesis procedure, the corresponding bare Ag/Ag_3PO_4 nanospecies could also be facilely synthesized via a parallel process.

1.4 Photocatalytic performance

For the photocatalytic experiments, photocatalysts typically involving 10 mg Ag/Ag_3PO_4 or Ag/Ag_3PO_4/GO nanospecies were dispersed in a 13.5 mL aqueous solution of methyl orange (MO, 20 mg L^{-1}), where a quartz cuvette was used as the reactor. A 500 W xenon arc lamp installed in a laboratory lamp housing system (CHF-XM35-500 W, Beijing Trusttech Co. Ltd., China) was employed as the light source. The light passed through a 10 cm waterfilter and a UV cutoff filter (>400 nm) before entering the reactor. The reaction system was kept for 30 min in a dark room to achieve an equilibrium adsorption state before visible-light irradiation. Aliquots of dispersion (0.4 mL) were taken out from the reaction system for the real-time sampling. For the evaluation of the photocatalytic activities, C is the concentration of MO dye at a real-time t, and C_0 is that in the MO solution immediately before it was kept in a dark room.

1.5 Apparatus and measurements

The scanning electron microscopy (SEM) measurements were carried out by using a Hitachi S-4800 system. The energy dispersive X-ray spectroscopy (EDX) was measured with a Horiba EMAX X-act energy dispersive spectroscopy that was attached to the Hitachi S-4800 system. JASCO UV-550 and JASCO IR-660 spectrometer were employed

for the UV-vis and FT-IR spectral measurements, respectively. X-ray diffraction (XRD) measurements were performed on a PANalytical X'Pert PRO instrument with Cu Kα radiation. The photodegradation of the MO dye was monitored by measuring the real-time UV-vis absorption of MO molecules at 463 nm using a JASCO UV-550 spectrometer. X-ray photoelectron spectroscopy (XPS) was performed on an ESCALab220i-XL electron spectrometer from VG Scientific using 300 W Al Kα radiation. The binding energies were referenced to the C 1s line at 284.8 eV from adventitious carbon. The Raman spectra were recorded on a Renishaw inVia plus Raman microscope using a 532 nm excitation laser. All the measurements were carried out at room temperature except noted.

2 Results and discussion

2.1 Synthesis and characterization of Ag/Ag_3PO_4 and GO hybridized Ag/Ag_3PO_4 nanospecies

Experimentally, Ag_3PO_4-based nanomaterials could be facilely manufactured by adding an aqueous solution of NaH_2PO_4 dropwise into an aqueous solution of CH_3COOAg via a deposition-precipitation method. The corresponding GO hybridized nanocomposites could also be thus obtained via an allied process, where an aqueous solution of GO nanosheets was added into an aqueous solution of CH_3-COOAg prior to the addition of the NaH_2PO_4 aqueous solution. Figure 1 shows the typical SEM images of the as-produced nanostructures. It can be seen that nanoparticles with an average size of ca. 300 nm could be obtained when GO is not involved during the synthesis procedure (Figure 1(a)). In contrast, as shown in Figure 1(b), nanostructures whose averaged size is ca. 150 nm and whose surface is enwrapped with silk-like nanosheets, are obtained when GO nanosheets are involved in the synthesis process. This suggests the possible formation of GO hybridized Ag_3PO_4-based nanocomposites. As proved in the following paragraphs, the successful hybridization could be verified by EDX, UV-vis, and FT-IR spectra of the obtained nanostructures.

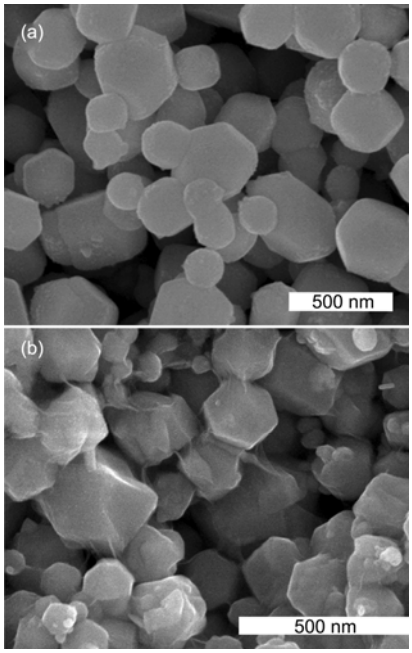

Figure 1 Typically SEM images of (a) the bare Ag/Ag_3PO_4 nanostructures and (b) the Ag/Ag_3PO_4/GO nanostructures.

It can be seen that compared with the bare Ag_3PO_4 nanostructures, the corresponding GO hybridized Ag_3PO_4 nanospecies display a smaller sized. This could be attributed to the existence of GO nanosheets in the synthesis system [28–30]. Structurally, GO nanospecies are atomic thick nanosheets of covalently organized lattice of carbon atoms, whose basal planes and edges are decorated with various oxygen-containing groups, such as hydroxyl, epoxide, carboxyl groups, etc [32,33]. Generally, the non-oxidized perfect graphene basal plane without only functional groups have intrinsic hydrophobic properties. In the case of GO nanosheets, the introduction of the covalently attached hydrophilic oxygen groups on their basal plane endows them with amphiphilic properties to some extent. Accordingly, this makes it possible that GO nanospecies could play a role as an unconventional polymeric surfactant in a colloid system [30,32,33]. On the other hand, from the viewpoint of nanofabrication, it has been demonstrated that the size of the produced nanostructures in a colloid system could be decreased by introducing polymeric surfactant molecules to the synthesis system [30,34–40]. These polymeric surfactant molecules are suggested to work as stabilizer or capping agents to hamper the further growth of the formed nanospecies, resulting in smaller nanostructures [30,34–40]. For example, it has recently been reported that the size of the Ag/AgCl nanoparticles could be decreased with the assistance of polymeric surfactant molecules, poly(vinyl pyrrolidone) [40]. On the basis of these well-documented understandings [30,32–40] and accompanied by our experimental facts, we suggest that in our system the GO nanosheet, an unconventional amphiphilic polymer, might work as capping agent or stabilizer to hamper the further growth of the Ag/Ag_3PO_4 nanoparticles, resulting in smaller size of the formed nanostructures. Similar results have been reported in other systems [28–30].

The components of the obtained nanostructures are primarily investigated by EDX analysis. As shown in Figure 2(a), oxygen, phosphorus and silver elements can be detected for the bare Ag_3PO_4-based nanoparticles. In the case of the GO-hybridized nanostructures, besides oxygen, phosphorus and silver elements, carbon element could also be detected distinctly, as shown in Figure 2(b). This result suggests the existence of GO species in the samples. Moreover, quantitative analysis shows that the atomic ratio between phosphorus and silver are both about 1∶3.5 for these two samples. This value is larger than the theoretic

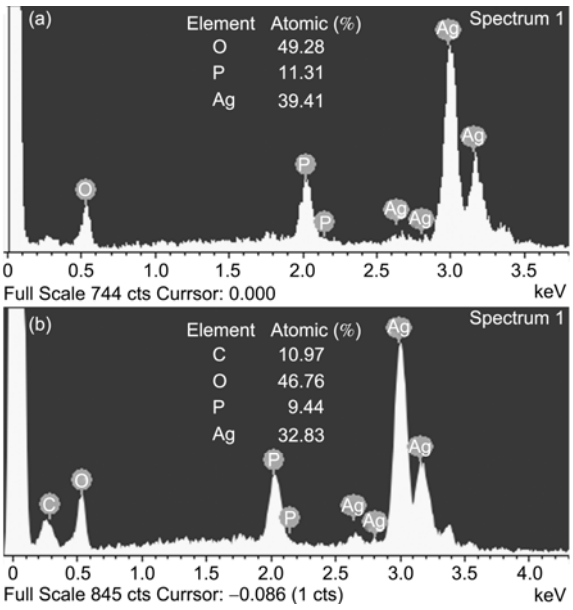

Figure 2 EDX elemental analysis of (a) the as-synthesized $Ag/A_{g3}PO_4$ and (b) Ag/Ag_3PO_4/GO nanospecies. The quantitative elemental analysis results in each case are also listed in the corresponding panels.

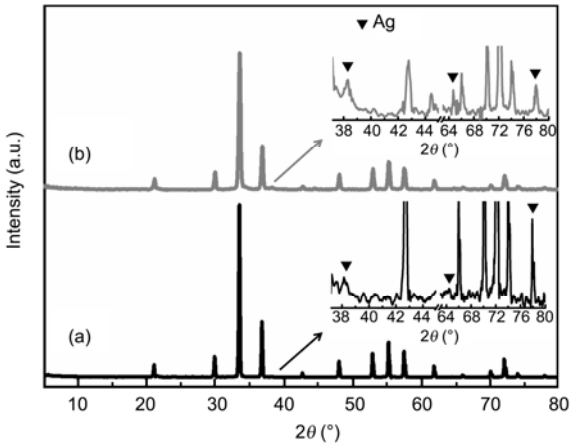

Figure 3 XRD spectra of (a) the bare Ag/Ag_3PO_4 and (b) Ag/Ag_3PO_4/GO nanostructures. Inset: the enlarged XRD patterns of Ag/Ag_3PO_4 and Ag/Ag_3PO_4/GO. The diffraction peaks ascribing to the metallic Ag species are marked with symbol ▼.

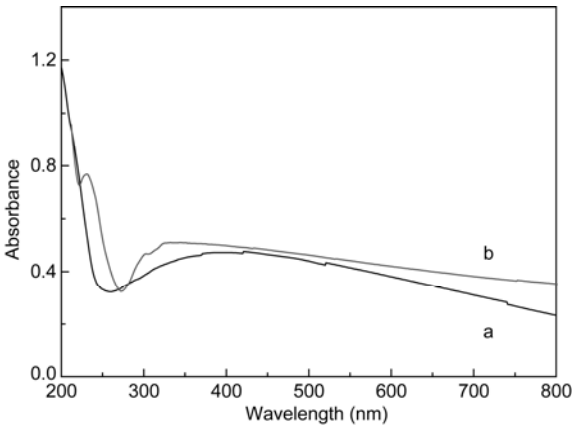

Figure 4 Typical UV-vis spectra of (a) Ag/Ag_3PO_4 and (b) Ag/Ag_3PO_4/GO nanospecies.

stoichiometric atomic ratio between phosphorus and silver in Ag_3PO_4, which should be 1∶3. These experimental facts suggest the possible generation of metallic Ag during our synthesis process, and thus resulting in the formation of Ag/Ag_3PO_4 or Ag/Ag_3PO_4/GO nanospecies.

To confirm this proposal, the XRD spectra of our products are investigated, as shown in Figure 3. It can be seen that both the samples display distinct diffraction peaks (2θ) at 21.1° (110), 29.9° (200), 33.5° (210), 36.8° (211), 42.7° (220), 48.0° (310), 52.9° (222), 55.2° (320), 57.5° (321), 61.8° (400), 66.0° (330), 70.1° (420), 72.1° (421), 74.0° (322), which correspond to the typical diffraction peaks of body-centred cubic structure of Ag_3PO_4 (JCPDS No. 06-0505) [16]. The weak diffraction peaks (2θ) at 38.2° (111), 44.3° (200), 64.5° (220), 77.9° (311) indicated by the inset of Figure 3 could be attributed to the metallic Ag (JCPDS No. 65–2871) [9]. These facts solidly confirms the formation of Ag/Ag_3PO_4 hybrid nanocomposites in these two systems. In the case of the GO hybridized system, negligible diffraction peaks attributing to GO nanosheets could be detected. Similar phenomenon has been disclosed from other GO-involved nanocomposites, where the absence of the diffraction peaks of GO is suggested to be owing to the low diffraction intensity of GO nanospecies [23].

Figure 4 shows the typical UV-visible spectra of the as-synthesized Ag/Ag_3PO_4 and Ag/Ag_3PO_4/GO nanostructures. It can be seen that both the samples display broad absorptions in the UV and visible regions. As known, the Ag_3PO_4 nanospecies could only show apparent absorptions in UV region, and in visible region with a wavelength shorter than 550 nm [16,17]. Accompanied by the above-mentioned information deduced from the EDX elemental analysis and the XRD spectra shown in Figures 2 and 3, the present result further confirms the existence of metallic Ag species in our samples, which could arouse surface plasmon resonance absorptions in the visible region [9,10,41]. At the same time, it can be seen from Figure 4 that the absorption spectrum of the Ag/Ag_3PO_4/GO nanocomposite displays a distinct absorption of GO nanosheets at ca. 231 nm, confirming the existence of GO nanospecies in this system [42].

In order to verify the hybridization of Ag/Ag_3PO_4 with GO nanosheets in Ag/Ag_3PO_4/GO system, their FT-IR together with that of powdery GO nanosheets were measured. As shown in Figure 5, the original powdery GO nanosheets displays a distinct vibration peak at 1737 cm^{-1}, which could be attributed to the characteristic vibration band of the C=O carbonyl stretching. For the bare Ag/Ag_3PO_4 nanospecies, there is negligible vibration band around this region. This is reasonable, since there exist no C=O carbonyl groups in Ag/Ag_3PO_4. In the case of the Ag/Ag_3PO_4/GO nanospecies,

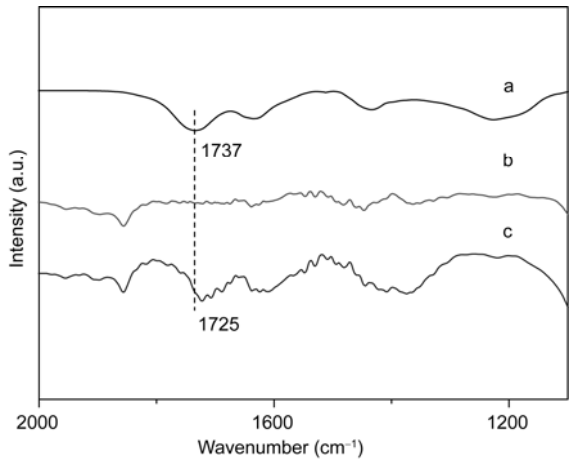

Figure 5 FT-IR spectra of (a) the original powdery GO nanosheets, (b) Ag/Ag_3PO_4, and (c) Ag/Ag_3PO_4/GO nanospecies.

the vibration peak of C=O carbonyl stretching shifts to 1725 cm^{-1}. Compared with the original powdery GO nanosheets, this peak displays a 12 cm^{-1} shift to the lower wavenumber, indicating the evident interaction between GO nanosheets and Ag/Ag_3PO_4 nanoparticles, and confirming the successful hybridization between these two components [28,43,44].

2.2 Photocatalytic performances of Ag/Ag_3PO_4-based nanostructures for the photodegradation of MO pollutant under visible-light irradiation

As mentioned in the above paragraphs, Ag/Ag_3PO_4-based nanostructures display broad surface plasmon resonance absorptions in the visible region (Figure 4), which is aroused by the metallic Ag species. This spectral feature makes our nanostructures might be photocatalytically active under visible-light irradiation. As shown in Figure 6(A), the photocatalytic performances of Ag/Ag_3PO_4 and Ag/Ag_3PO_4/GO nanostructures are investigated by photodegradation of MO dye under visible-light irradiation. Experimentally, a dark adsorption experiment was performed to achieve an equilibrium adsorption state prior to the irradiation. For comparison, photodegradation experiments were also carried out without catalysts, where it can be seen that negligible decomposition of MO dyes occurred. This suggests that the self-sensitized photodegradation of MO could hardly occur under our experimental conditions.

When the Ag/Ag_3PO_4 nanospecies are employed as photocatalysts, about 78% MO molecules are decomposed within 24 min. In contrast, when Ag/Ag_3PO_4/GO nanostructures are instead used as catalysts, about 95% MO pollutants are decomposed under the similar experimental conditions. These results indicate that Ag/Ag_3PO_4-based nanostructures could be used as visible-light-driven plasmonic photocatalysts for the photodegradation of MO pollutant. At the same time, it can be seen that the photocatalytic performance of our Ag/Ag_3PO_4 could be distinctly enhanced by ca. 17% via hybridization with GO nanosheets. As plotted in Figure 6(B), $\ln(C/C_0)$ and the reaction time (t) exhibits a linear relationship, indicating that the decomposition reaction of MO molecules follows the first-order kinetics:

$$-\mathrm{d}C/\mathrm{d}t = kC,$$

where C is concentration of the MO molecules, t is reaction time, and k is the rate constant. The rate constant of Ag/Ag_3PO_4 and Ag/Ag_3PO_4/GO based catalysts are determined to be 0.063 and 0.119 min^{-1}, respectively. Thus, it can be seen that efficiency of the Ag/Ag_3PO_4 based photo

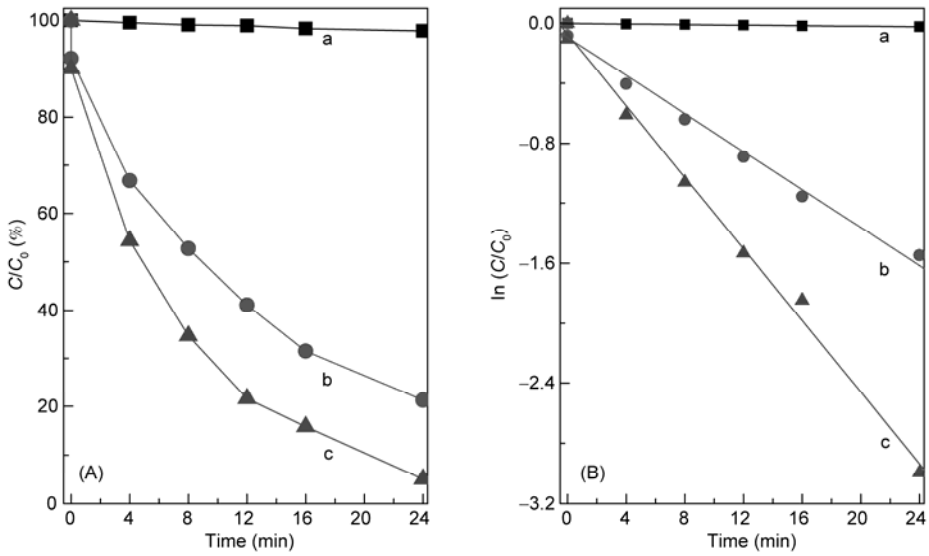

Figure 6 (A) Photocatalytic activity and (B) kinetic linear simulation curves of the Ag/Ag_3PO_4-based plasmonic photocatalysts for the photodegradation of MO pollutant under visible-light irradiations. (a) A blank experiment, where no catalyst is used; the employed catalysts for curves (b) and (c) are bare Ag/Ag_3PO_4 and Ag/Ag_3PO_4/GO, respectively.

catalyst has been ca. 2 times enhanced upon hybridization with GO.

As known, an efficient charge separation/transfer or a suppressed recombination of electron-hole pairs is one of the most crucial factors for the enhancement of the photocatalytic activities [1–8,23]. To propose an explanation for the enhanced photocatalytic performance observed from the $Ag/Ag_3PO_4/GO$ systems. The XPS of Ag/Ag_3PO_4 and $Ag/Ag_3PO_4/GO$ hybrid nanocomposites were examined. As shown in Figure 7, for the bare Ag/Ag_3PO_4 nanostructures, two bands at ca. 373.5 and 367.5 eV, which can be attributed to Ag $3d_{3/2}$ and Ag $3d_{5/2}$ binding energies, respectively, could be observed. These two bands could be further deconvoluted into two sets of peaks at 373.5, 374.2 eV and 367.5, 368.3 eV, wherein those at 374.2 and 368.3 eV are ascribed to the metallic Ag^0 of Ag/Ag_3PO_4, and those at 373.5 and 367.5 eV are attributed to Ag^+, respectively [28,45,46]. In the cases of the GO-involved nanostructures, $Ag/Ag_3PO_4/GO$, the Ag $3d_{5/2}$ and Ag $3d_{3/2}$ peaks shift to higher binding energies to 368 and 374 eV, respectively. The deconvolution of these two bands gives out peaks at 368, 368.9 eV and 374, 374.8 eV, respectively. Those at 368 and 374 eV could be ascribed to the Ag^+ of Ag_3PO_4, while those at 368.9 and 374.8 eV are ascribed to the metallic Ag^0. The calculated surface mole ratio of metallic Ag^0 to Ag^+ in Ag/Ag_3PO_4 and $Ag/Ag_3PO_4/GO$ nanospecies is both ca. 1∶6. On one hand, these results further solidly confirm the existence of metallic Ag^0 in our Ag/Ag_3PO_4-based nanostructures, as suggested by the EDX, XRD, and UV-vis spectra. On the other hand, the higher binding energy of Ag species observed from the $Ag/Ag_3PO_4/GO$ system compared with that detected from the bare Ag/Ag_3PO_4 system suggests that the Ag/Ag_3PO_4 of $Ag/Ag_3PO_4/GO$ works as electron donor in the GO hybridized system, while GO nanosheet acts as electron acceptor [28,47].

To further confirm this proposal, the Raman spectra of $Ag/Ag_3PO_4/GO$ together with that of the original powdery GO nanosheets were investigated. As shown in Figure 8, it

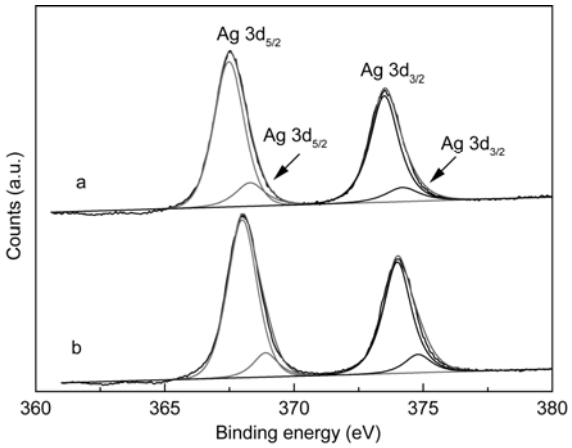

Figure 7 XPS spectra of (a) Ag 3d of Ag/Ag_3PO_4 and (b) $Ag/Ag_3PO_4/GO$ nanostructures.

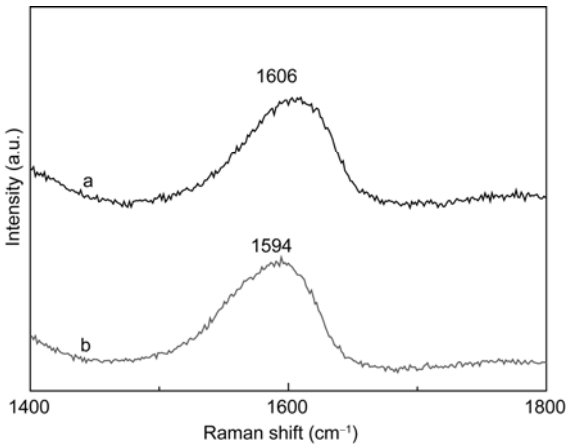

Figure 8 Raman spectra of the G band of (a) the powdery GO naonsheets and (b) the $Ag/Ag_3PO_4/GO$ nanostructures.

can been seen that a G band at ca. 1606 cm^{-1}, which is typical Raman features of GO nanosheets, could be observed from the original powdery GO nanospecies [28]. On the other hand, the G band shifts by ca. 12 cm^{-1} to a lower frequency at 1594 cm^{-1} for the $Ag/Ag_3PO_4/GO$ nanocomposites. Generally, it has been proved that the G band of GO nanosheets shifts to lower frequency when it is hybridized with an electron donor component, while it shifts to higher frequency when an electron acceptor component is hybridized [28,48–50]. Accompanied by the information deduced from the XPS spectra, the present Raman spectra further confirm that in our $Ag/Ag_3PO_4/GO$ system, GO works as electron acceptor while Ag/Ag_3PO_4 acts as electron donor. Consequently, it is reasonable that compared with the bare Ag/Ag_3PO_4 system, a more efficient charge separation/transfer and a suppressed recombination of electron-hole pairs could be achieved in our $Ag/Ag_3PO_4/GO$ system, resulting in the observed enhanced photocatalytic activity [28–30].

As known, besides the charge separation/transfer or the recombination of electron-hole pairs, the size of the catalysts is another factor that might affect the catalytic activity, where it has been demonstrated that the smaller the size of the catalysts, the higher of their catalytic activity [17,28,51]. This is suggested to be owing to the existence of more catalytically active sites in the smaller catalysts [51]. As described in the above paragraphs, we note that the size of Ag/Ag_3PO_4 in the $Ag/Ag_3PO_4/GO$ system is distinctly smaller than that in the bare Ag/Ag_3PO_4 system, as shown in Figure 1. Thus, we propose that this factor might also contribute partially to the enhanced catalytic performance of our $Ag/Ag_3PO_4/GO$ system.

3 Conclusion

In conclusion, we have shown in the present new efforts that Ag/Ag_3PO_4 nanospecies and the corresponding GO

hybridized nanocomposites, $Ag/Ag_3PO_4/GO$, could be facilely produced *via* a deposition-precipitation method. These nanostructures could be employed as visible-light-driven plasmonic photocatalysts for the photodegradatoin of MO pollutant. Compared with the bare Ag/Ag_3PO_4 nanostructures, the GO-involved nanohybrids display distinctly enhanced photocatalytic activity for the degradation of MO pollutant under visible-light irradiations. It is suggested that the hybridization of GO nanosheets facilitates a more efficient charge separation/transfer or a suppressed recombination of electron-hole pairs in the $Ag/Ag_3PO_4/GO$ system. At the same time, the introduction of GO nanosheets in the synthesis system, promotes a smaller size of the assembled Ag/Ag_3PO_4 nanospecies. These factors, all of which are a result of hybridization of GO nanosheets, are suggested to be responsible for the enhancement of the photocatalytic performance of $Ag/Ag_3PO_4/GO$. Our investigation might initiate new opportunities for the manufacturing of visible-ight-energized Ag_3PO_4-based photocatalysts with enhanced catalytic activities.

This work was supported by the National Natural Science Foundation of China (20873159, 21021003 and 91027042), and the Ministry of Science and Technology of China (2011CB932301).

1 Hoffmann M R, Martin S T, Choi W, et al. Environmental applications of semiconductor photocatalysis. Chem Rev, 1995, 95: 69–96
2 Byrne J A, Fernandez-Ibañez P A, Dunlop P S M, et al. Photocatalytic enhancement for solar disinfection of water: A review. Int J Photoenergy, 2011, 2011: 798051
3 Chen C C, Ma W H, Zhao J C. Semiconductor-mediated photodegradation of pollutants under visible-light irradiation. Chem Soc Rev, 2010, 39: 4206–4219
4 Zhang J L, Wu Y M, Xing M Y, et al. Development of modified N doped TiO_2 photocatalyst with metals, nonmetals and metal oxides. Energy Environ Sci, 2010, 3: 715–726
5 Linsebigler A L, Lu G Q, Yates Jr J T. Photocatalysis on TiO_2 surfaces: Principles, mechanisms, and selected results. Chem Rev, 1995, 95: 735–758
6 Carp O, Huisman C L, Reller A. Photoinduced reactivity of titanium dioxide. Prog Solid State Chem, 2004, 32: 33–177
7 Chen X B, Mao S S. Titanium dioxide nanomaterials: Synthesis, properties, modifications, and applications. Chem Rev, 2007, 107: 2891–2959
8 Sin J C, Lam S M, Mohamed A R, et al. Degrading endocrine disrupting chemicals from wastewater by TiO_2 photocatalysis: A review. Int J Photoenergy, 2012, 2012: 185159
9 Wang P, Huang B B, Qin X Y, et al. Ag@AgCl: A highly efficient and stable photocatalyst active under visible light. Angew Chem Int Ed, 2008, 47: 7931–7933
10 Wang P, Huang B B, Zhang X Y, et al. Highly efficient visible-light plasmonic photocatalyst Ag@AgBr. Chem Eur J, 2009, 15: 1821–1824
11 Wang X F, Li S F, Yu H G, et al. Ag_2O as a new visible-light photocatalyst: Self-stability and high photocatalytic activity. Chem Eur J, 2011, 17: 7777–7780
12 Ouyang S X, Kikugawa N, Chen D, et al. Systematical study on photocatalytic properties of $AgMO_2$ (M = Al, Ga, In): Effects of chemical compositions, crystal structures, and electronic structures. J Phys Chem C, 2009, 113: 1560– 1566
13 Shi H F, Li Z S, Kou J H, et al. Facile synthesis of single-crystalline $Ag_2V_4O_{11}$ nanotube material as a novel visible-light-sensitive photocatalyst. J Phys Chem C, 2011, 115: 145–151
14 Tong H, Ouyang S X, Bi Y P, et al. Nano-photocatalytic materials: Possibilities and challenges. Adv Mater, 2012, 24: 229–251
15 Yi Z G, Ye J H, Kikugawa N, et al. An orthophosphate semiconductor with photooxidation properties under visible-light irradiation. Nat Mater, 2010, 9: 559–564
16 Bi Y P, Ouyang S X, Umezawa N, et al. Facet effect of single-crystalline Ag_3PO_4 sub-microcrystals on photocatalytic properties. J Am Chem Soc, 2011, 133: 6490–6492
17 Dinh C T, Nguyen T D, Kleitz F, et al. Large-scale synthesis of uniform silver orthophosphate colloidal nanocrystals exhibiting high visible light photocatalytic activity. Chem Commun, 2011, 47: 7797–7799
18 Bi Y P, Ouyang S X, Cao J Y, et al. Facile synthesis of rhombic dodecahedral AgX/Ag_3PO_4 (X = Cl, Br, I) heterocrystals with enhanced photocatalytic properties and stabilities. Phys Chem Chem Phys, 2011, 13: 10071–10075
19 Liu Y P, Fang L, Lu H D, et al. Highly efficient and stable Ag/Ag_3PO_4 plasmonic photocatalyst in visible light. Catal Commun, 2012, 17: 200–204
20 Stankovich S, Dikin D A, Dommett G H B, et al. Graphene-based composite materials. Nature, 2006, 442: 282–286
21 Zhu Y W, Murali S, Cai W W, et al. Graphene and graphene oxide: Synthesis, properties, and applications. Adv Mater, 2010, 22: 3906–3924
22 Dreyer D R, Park S, Bielawski C W, et al. The chemistry of graphene oxide. Chem Soc Rev, 2010, 39: 228–240
23 Zhang H, Lü X J, Li Y M, et al. P25-graphene composite as a high performance photocatalyst. ACS Nano, 2010, 4: 380–386
24 An X Q, Yu J C. Graphene-based photocatalytic composites. RSC Adv, 2011, 1: 1426–1434
25 Xiang Q J, Yu J G, Jaroniec, M. Graphene-based semiconductor photocatalysts. Chem Soc Rev, 2012, 41: 782–796
26 Bai S, Shen X P. Graphene-inorganic nanocomposites. RSC Adv, 2012, 2: 64–98
27 Lü K, Zhao G X, Wang X K. A brief review of graphene-based material synthesis and its application in environmental pollution management. Chin Sci Bull, 2012, 57: 1223–1234
28 Zhu M S, Chen P L, Liu M H. Graphene oxide enwrapped Ag/AgX (X = Br, Cl) nanocomposite as a highly efficient visible-light plasmonic photocatalyst. ACS Nano, 2011, 5: 4529–4536
29 Zhu M S, Chen P L, Liu M H. Sunlight-driven plasmonic photocatalysts based on Ag/AgCl nanostructures synthesized via an oil-in-water medium: Enhanced catalytic performance by morphology selection. J Mater Chem, 2011, 21: 16413–16419
30 Zhu M S, Chen P L, Liu M H. Ag/AgBr/graphene oxide nanocomposite synthesized via oil/water and water/oil microemulsions: A comparison of sunlight energized plasmonic photocatalytic activity. Langmuir, 2012, 28: 3385–3390
31 Zhang H, Fan X F, Quan X, et al. Graphene sheets grafted Ag@AgCl hybrid with enhanced plasmonic photocatalytic activity under visible light. Environ Sci Technol, 2011, 45: 5731–5736
32 Kim J, Cote L J, Kim F, et al. Graphene oxide sheets at interfaces. J Am Chem Soc, 2010, 132: 8180–8186
33 Bai H, Li C, Shi G Q. Functional composite materials based on chemically converted graphene. Adv Mater, 2011, 23: 1089–1115
34 Daniel M C, Astruc D. Gold nanoparticles: Assembly, supramolecular chemistry, quantum-size-related properties, and applications toward biology, catalysis, and nanotechnology. Chem Rev, 2004, 104: 293–346
35 Hossain M J, Tsunoyama H, Yamauchi M, et al. High-yield synthesis of PVP-stabilized small Pt clusters by microfluidic method. Catal Today, 2012, 183: 101–107
36 Yu W Y, Tu W X, Liu H F. Synthesis of nanoscale platinum colloids by microwave dielectric heating. Langmuir, 1999, 15: 6–9
37 Teranishi T, Hosoe M, Tanaka T, et al. Size control of monodispersed Pt nanoparticles and their 2D organization by electrophoretic deposition. J Phys Chem B, 1999, 103: 3818–3827
38 Wang Y, Ren J W, Deng K, et al. Preparation of tractable platinum,

rhodium, and ruthenium nanoclusters with small particle size in organic media. Chem Mater, 2000, 12: 1622–1627
39 Zeng J, Zheng Y Q, Rycenga M, et al. Controlling the shapes of silver nanocrystals with different capping agents. J Am Chem Soc, 2010, 132: 8552–8553
40 An C H, Peng S, Sun Y G. Facile synthesis of sunlight-driven AgCl:Ag plasmonic nanophotocatalyst. Adv Mater, 2010, 22: 2570–2574
41 Rycenga M, Cobley C M, Zeng J, et al. Controlling the synthesis and assembly of silver nanostructures for plasmonic applications. Chem Rev, 2011, 111: 3669–3712
42 Li D, Müller M B, Gilje S, et al. Processable aqueous dispersions of graphene nanosheets. Nat Nanotechnol, 2008, 3: 101–105
43 Zhu M S, Li Z, Du Y K, et al. Stable and efficient homogeneous photocatalytic H_2 evolution based on water soluble pyrenetetrasulfonic acid functionalized platinum nanocomposites. ChemCatChem, 2012, 4: 112–117
44 Petroski J, El-Sayed M A. FTIR study of the adsorption of the capping material to different platinum nanoparticle shapes. J Phys Chem A, 2003, 107: 8371–8375
45 Wang P, Huang B B, Qin X Y, et al. Ag/AgBr/$WO_3 \cdot H_2O$: Visible-light photocatalyst for bacteria destruction. Inorg Chem, 2009, 48: 10697–10702
46 Wang P, Huang B B, Lou Z Z, et al. Synthesis of highly efficient Ag@AgCl plasmonic photocatalysts with various structures. Chem Eur J, 2010, 16: 538–544
47 Briggs D. Handbook of X-ray and Ultraviolet Photoelectron Spectroscopy. London: Hyden & Son, 1977
48 Xu Y X, Wu Q, Sun Y Q, et al. Three-dimensional self-assembly of graphene oxide and DNA into multifunctional hydrogels. ACS Nano, 2010, 4: 7358–7362
49 Ghosh A, Rao K V, George S J, et al. Noncovalent functionalization, exfoliation, and solubilization of graphene in water by employing a fluorescent coronene carboxylate. Chem Eur J, 2010, 16: 2700–2704
50 Das A, Pisana S, Chakraborty B, et al. Monitoring dopants by Raman scattering in an electrochemically top-gated graphene transistor. Nat Nanotechnol, 2008, 3: 210–215
51 Chen J Y, Lim B, Lee E P, et al. Shape-controlled synthesis of platinum nanocrystals for catalytic and electrocatalytic applications. Nano Today, 2009, 4: 81–95